

Incremental Passivity Control in Multilevel Cascaded H-Bridge Converters

Ezequiel Rodriguez, *Student Member, IEEE*, Ramon Leyva, *Member, IEEE*, Glen Farivar, *Member, IEEE*, Hossein Dehghani Tafti, *Member, IEEE*, Christopher D. Townsend, *Member, IEEE*, and Josep Pou, *Fellow, IEEE*

Abstract—A low-capacitance static compensator (LC-StatCom) based on a cascaded H-bridge (CHB) multilevel converter can be an efficient and low-cost solution for reactive power compensation in power grids. However, the reduced capacitance, and therefore faster capacitor voltage dynamics, makes it challenging to control it. Classical cascade control schemes, in which the bandwidths associated with the inner current loop and the outer capacitor voltage loop need to be separated enough, are the most reported approaches. Nevertheless, for the LC-StatCom case, the voltage loop can be almost as fast as that one of the current loop. For this reason, this paper proposes a control approach that does not separate voltage and current dynamics. Concretely, we propose a multi-input linear time-variant control law, based on incremental passivity theory for CHB multilevel converters. The proposed control guarantees stability despite saturation in the control signal. In addition, it provides capacitor voltage balance without the need to use a specific balancing stage. The paper, first, reviews the average model of the converter and then, analyses the steady-state dynamic behaviour to determine the desired and coherent reference signals. Then, it applies an incremental passivity control approach to drive the LC-StatCom state variables to the desired references. After introducing the proposed control law, experimental results on a seven-level 1-kVA CHB LC-StatCom are shown to demonstrate its excellent performance in steady-state and transients.

Index Terms—Bilinear system control, cascaded H-bridge (CHB), incremental passivity, multi-input global tracking, multilevel converter, static compensator (STATCOM)

I. INTRODUCTION

Static compensators (StatComs) play an important role in the reliable operation of modern transmission lines [1], [2]. They ensure reactive power balance and grid voltage stability, despite variations in the load and hence, facilitate grid integration of renewable energy resources [3], [4]. The cascaded H-bridge (CHB) multilevel converter is the leading technology for medium/high power StatComs, due to its superior efficiency, modularity, and harmonic and dynamic performances [5], [6]. The circuit diagram of a CHB power converter arm is shown in Fig. 1(a).

The recently proposed low-capacitance StatCom (LC-StatCom) [7]–[12] is able to reduce the total capacitance by more than 50%, compared to conventional technology, by allowing large low-frequency voltage oscillation on the capacitors. This enables: 1) a significant reduction in the capacitor size requirements, which lowers cost, weight, and volume of the system; 2) the use of film or ceramic capacitors, instead of high power-density electrolytic capacitors, which enhances

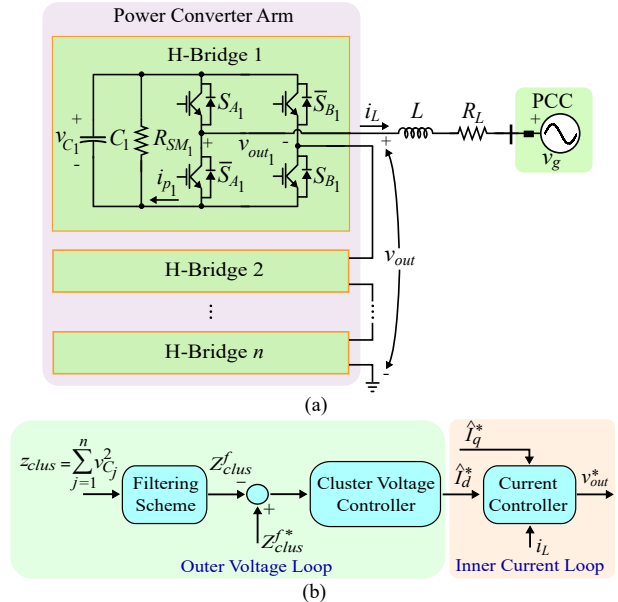


Fig. 1. CHB power converter arm. (a) Circuit diagram and (b) classical cascade control block diagram.

the reliability of the converter [13]–[15]; 3) improvements in converter efficiency and harmonic performance, specially when injecting close to full capacitive reactive power to the grid [16], [17]. Superior efficiency is achieved due to the lower capacitor voltage and the strong dependency between switching loss and the voltage at the time of each switching event. The time-varying capacitor voltage also results in a shaped pulse-width modulated (PWM) converter voltage with higher spectral quality. Despite these advantages, the LC-StatCom technology is still under development and many research questions remain unanswered, particularly those related to controller issues, as its ability to reject undesired disturbances quickly.

Conventional control strategies for CHB-StatComs, such as those reported in [5], [18], presume capacitors large enough that their voltages could be considered constant, or almost constant. Therefore, voltage dynamics can be separated from the current dynamics. Such an assumption is not strictly valid in the LC-StatCom and hence, implementation of a conventional cascade control scheme can lead to poor and

slow transient responses (and saturation effects) that do not meet the grid requirements. Addressing this control dilemma was not the focus of previous studies on the LC-StatCom, where the slow dynamic was considered an accepted drawback [7], [12]. Fig. 1(b) illustrates, using a simplified control block diagram, the classical cascade control scheme based on the instantaneous power theory. The square-sum-capacitor-voltages in the power converter arm is denoted as $z_{clus} = \sum_{j=1}^n v_{C_j}^2$, where v_{C_j} is the capacitor voltage in the j^{th} H-bridge, and $j \in \{1, 2, \dots, n\}$ is the H-bridge index in the converter arm, as shown in Fig. 1(a). The aim of the outer voltage loop is to regulate the dc component of the square-sum-capacitor-voltages to the reference Z_{clus}^{f*} . This aim is achieved by calculating the required active power component of the arm current \hat{I}_d^* , which together with its reactive counterpart \hat{I}_q^* , constitute the current reference for the inner current loop. Then, the inner current loop calculates the converter voltage reference v_{out}^* that meets the current tracking objective.

Despite the inherent nonlinear time-varying multi-input nature of the multilevel converter, most of the literature uses a reduced-order model of the converter [19], which assumes that the voltages in the capacitors are balanced. The balanced assumption involves that the converter requires the use of an inter-cell voltage balancing scheme [20], [21]. The time-varying nature of the converter is due to the fact that the grid voltage is sinusoidal and that the desired injected StatCom current is also a sinusoidal waveform. Many authors deal with the time-varying nature of the converter by using the well-known Park transformation, which leads to a linear model for the current state variable. Nevertheless, the dynamics associated with the capacitor voltages still remain nonlinear time-varying. Thus, as discussed above, the traditional cascade approach has been proposed by many authors to deal with this control problem. The inner loop, which is basically linear, is handled first, and then the design of the outer loop that is intrinsically nonlinear. Unlike this two-loop approach, the authors propose to handle the whole design as a nonlinear multi-variate control problem. Thus, avoiding the necessity of having separated bandwidths associated with each loop.

Among the possible nonlinear time-varying control techniques to be used, incremental passivity based control is attractive because it can guarantee stability despite control saturation. Dealing with control saturation is very important in LC-StatCom applications since it appears when the capacitor voltages are not high enough during transients. Motivated by the above, this paper introduces a multi-input time-varying control law based on the passivity concept for the LC-StatCom. The passivity approach was studied in [22]–[24] for controlling dc-dc converters. However, its use in ac multilevel conversion, and specifically for the CHB converter, is still in an early stage. In [25], [26], a passivity-based control was presented for a modular multilevel converter. However, an additional inter-cell capacitor voltage balance scheme was required. In contrast, the proposed multi-input passivity approach controls each H-bridge with a different control law and hence, the voltage balancing is a direct consequence

of the tracking objectives. In [27], a passivity-based control implements the current regulator of a star-connected CHB-StatCom in the rotating dq frame, in which the active power component of the current reference is modified by an outer, lower bandwidth, control loop that regulates the total of all capacitor voltages. In contrast, as it was mentioned above, the proposed passivity approach integrates both the current control and outer capacitor voltage control in one stage, providing a high bandwidth current and capacitor voltage control. Besides, the proposed control scheme effectively maintains a maximum limit on capacitor voltages, as required by the LC-StatCom operating principle [7]. Finally, an important feature of the proposed control approach is that it results in a linear control law in spite of the inherently bilinear nature of the system.

The rest of this paper is organised as follows. First, the CHB converter model is reviewed in Section II, where a circuital model of the averaged dynamics is also presented. In Section III, the design of the reference signals, based on the steady-state behaviour, is addressed with consideration of the loss parameters. Also, constraints in the capacitor voltages for safe and stable operation are analysed in this section. The proposed control law, which is multivariate and adapted to the CHB converter, is derived in Section IV. Section V describes the scaled-down experimental setup and reports experimental results, which show excellent capacitor voltage balancing capability, and transient and steady-state performance. Finally, Section VI summarises and concludes the main ideas in the paper.

II. CASCADED H-BRIDGE CONVERTER MODEL

This section reviews the CHB converter topology, its state variables, and an exact piecewise continuous state-space model. Then, the averaged model of the system is derived, which establishes the notations used in the analysis of the proposed incremental passivity control law.

The converter topology, shown in Fig. 1(a), represents an arm of the CHB converter. A filtering inductor L is interfacing the power converter with the grid. The power converter arm consists of n series-connected H-bridges. Each H-bridge is made up of a floating capacitor C_j at the dc-side, and four semiconductor power switches, which form an H-bridge structure with three possible output voltage levels.

The inductor current i_L , and the n capacitor voltages $v_{C_1}, v_{C_2}, \dots, v_{C_n}$, are the state variables for describing the dynamic behaviour of the CHB converter, shown in Fig. 1(a). The variable v_g represents the point of common coupling (PCC) voltage (the point at which the StatCom connects to the network). The set of discontinuous switching positions of each H-bridge S_j are taken as the control inputs. The state variables are grouped in the vector $\mathbf{x} \in \mathbb{R}^{n+1}$, and the control inputs are combined in the vector $\mathbf{u} \in \mathbb{R}^n$, as:

$$\mathbf{x}(t) = [i_L(t) \ v_{C_1}(t) \ v_{C_2}(t) \ \dots \ v_{C_n}(t)]^T \quad (1)$$

$$\mathbf{u}(t) = [S_1(t) \ S_2(t) \ \dots \ S_n(t)]^T, \quad (2)$$

where the discrete term S_j that drives the j^{th} H-bridge belongs to the set $\{-1, 0, 1\}$, $\forall j \in \{1, 2, \dots, n\}$. The losses of each H-bridge are modeled with a resistance of value R_{SM_j} in parallel with the capacitor C_j , whereas the parasitic resistance of the filtering inductor L is modeled with the series resistance R_L , as depicted in Fig. 1(a).

The ac- and dc-sides of the converter arm are related by the discontinuous control function S_j as:

$$v_{out}(t) = \sum_{j=1}^n v_{C_j}(t) S_j(t) \quad (3)$$

$$i_{p_j}(t) = i_L(t) S_j(t), \quad (4)$$

where $\forall j \in \{1, 2, \dots, n\}$. The variable v_{out} is the PWM converter output voltage, and i_{p_j} is the dc-side current on the j^{th} H-bridge. It can be noted that both v_{out} and i_{p_j} are piecewise continuous time functions. The sum of capacitor voltages in the converter arm is defined as the cluster voltage v_{clus} , i.e., $v_{clus} = \sum_{j=1}^n v_{C_j}$, and it will be used to express the capacitor voltage reference signals to track, in next sections. Note that v_{clus} is independent of the switching positions S_j .

The dynamic model of the converter, considering independent switching of each H-bridge, corresponds to the following $n+1$ differential equations:

$$L \dot{i}_L(t) = -R_L i_L(t) + v_{out}(t) - v_g(t) \quad (5)$$

$$C_j \dot{v}_{C_j}(t) = -i_{p_j}(t) - \frac{v_{C_j}(t)}{R_{SM_j}}, \quad (6)$$

where $\forall j \in \{1, 2, \dots, n\}$. These equations can be grouped as the following matrix representation:

$$\begin{bmatrix} \dot{i}_L \\ \dot{v}_{C_1} \\ \dot{v}_{C_2} \\ \vdots \\ \dot{v}_{C_n} \end{bmatrix} = \begin{bmatrix} \gamma_L & \frac{S_1}{L} & \frac{S_2}{L} & \cdots & \frac{S_n}{L} \\ -\frac{S_1}{C_1} & \gamma_{C_1} & 0 & \cdots & 0 \\ -\frac{S_2}{C_2} & 0 & \gamma_{C_2} & \cdots & 0 \\ \vdots & \vdots & \vdots & \ddots & \vdots \\ -\frac{S_n}{C_n} & 0 & 0 & \cdots & \gamma_{C_n} \end{bmatrix} \begin{bmatrix} i_L \\ v_{C_1} \\ v_{C_2} \\ \vdots \\ v_{C_n} \end{bmatrix} + \begin{bmatrix} -\frac{v_g}{L} \\ 0 \\ 0 \\ \vdots \\ 0 \end{bmatrix}, \quad (7)$$

or equivalently,

$$\dot{\mathbf{x}}(t) = \left(\mathcal{A} + \sum_{j=1}^n \mathcal{B}_j S_j(t) \right) \mathbf{x}(t) + \mathcal{C} v_g(t). \quad (8)$$

Note that the time dependence notation is avoided in (7) for the sake of simplicity and readability.

The real constant matrices $\mathcal{A} \in \mathbb{R}^{(n+1) \times (n+1)}$, $\mathcal{B}_j \in \mathbb{R}^{(n+1) \times (n+1)}$, $\mathcal{C} \in \mathbb{R}^{(n+1) \times 1}$ are equal to:

$$\mathcal{A} = \begin{bmatrix} \gamma_L & 0 & 0 & \cdots & 0 \\ 0 & \gamma_{C_1} & 0 & \cdots & 0 \\ 0 & 0 & \gamma_{C_2} & \cdots & 0 \\ \vdots & \vdots & \vdots & \ddots & \vdots \\ 0 & 0 & 0 & \cdots & \gamma_{C_n} \end{bmatrix}, \quad \mathcal{C} = \begin{bmatrix} -\frac{1}{L} \\ 0 \\ \vdots \\ 0 \end{bmatrix},$$

$$\mathcal{B}_j = \begin{bmatrix} \beta_{1,1}^j & \cdots & \beta_{1,n+1}^j \\ \vdots & \ddots & \vdots \\ \beta_{n+1,1}^j & \cdots & \beta_{n+1,n+1}^j \end{bmatrix}, \quad (9)$$

with $\gamma_L = -R_L/L$, and $\gamma_{C_j} = -1/(R_{SM_j} C_j)$. The elements of matrices \mathcal{B}_j are $\beta_{1,j+1}^j = 1/L$, $\beta_{j+1,1}^j = -1/C_j$, and $\beta_{k,l}^j = 0 \forall (k \neq j+1, l \neq 1)$ and $\forall (k \neq 1, l \neq j+1)$.

It is noted that the control input is multiplied by the state-space variables, hence the state model results in bilinear behaviour [28]. Thus, the proposed CHB converter model is nonlinear, with dimension $n+1$, and with n control inputs. In addition, these state-space variables are time-varying and piecewise continuous due to the switching nature of the converter.

The switching model in (8) can be approximated by an averaged model with the continuous state variables,

$$\dot{\bar{\mathbf{x}}}(t) = \left(\mathcal{A} + \sum_{j=1}^n \mathcal{B}_j \delta_j(t) \right) \bar{\mathbf{x}}(t) + \mathcal{C} v_g(t), \quad (10)$$

where $\bar{\mathbf{x}} = [\bar{i}_L \ \bar{v}_{C_1} \ \bar{v}_{C_2} \ \cdots \ \bar{v}_{C_n}]^T$ represents the averaged current and voltage state variables. The averaged control input of the modulator δ_j is

$$\delta_j(t) = \frac{1}{T_{sw}} \int_{t-T_{sw}}^t S_j(\tau) d\tau \in [-1, 1], \quad (11)$$

where $\forall j \in \{1, 2, \dots, n\}$. This parameter is adjusted by the proposed controller in order to track the state reference. The switching period T_{sw} is assumed much lower than the converter system time-constants, and significantly lower than $2\pi/\omega_{r_j}$, where $\omega_{r_j} = 1/\sqrt{LC_j}$ is the j^{th} resonant frequency of the j^{th} H-bridge.

This continuous average state-space representation form can be visualised as the circuit shown in Fig. 2. As it can be seen, each H-bridge in the converter arm acts as a variable ratio ideal transformer in the averaged model.

This section has stated the notations of the averaged model, which will be used in the following sections to derive the proposed control law for the CHB converter.

III. CHB STEADY-STATE REFERENCE SIGNALS

In this section, steady-state reference signals are defined and the design constraints are introduced.

Fig. 3 depicts the control block diagram of the proposed incremental passivity-based control applied to a CHB converter. The converter is synchronised with the PCC voltage

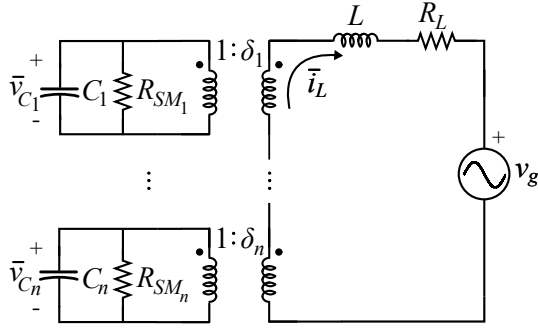


Fig. 2. Averaged-model equivalent circuit of a CHB power converter arm.

by using a phase-locked loop (PLL) to track the angle $\omega_g t$. Subsequently, based on the knowledge of the PCC voltage and desired current to compensate reactive power \bar{i}_L^* , the reference signals for \bar{v}_{C_j} and δ_j , denoted as $\bar{v}_{C_j}^*$ and δ_j^* , respectively, are calculated using the proposed steady-state reference generation algorithm. Finally, a passivity-based multi-input control strategy is developed to generate the averaged control inputs of the modulator δ_j , which are fed into a phase-shifted carrier PWM (PSC-PWM) block [29], [30] to generate the switching signals.

A. Coherent Reference Expressions

It is important to have coherent time-varying references in modular multilevel converters, specially when using small capacitance values where the capacitor voltages consist of several harmonic components, because the control loop performance is highly reliant on the reference signals design [25], [31], [32]. In order to derive coherent expressions for the capacitor voltages and averaged control inputs of the modulator, the following expressions are used for a desired average load current reference \bar{i}_L^* and a given PCC voltage v_g :

$$\bar{i}_L^*(t) = \hat{I}_L^* \sin(\omega_g t + \varphi^*) \quad (12)$$

$$v_g(t) = \hat{V}_g \sin(\omega_g t). \quad (13)$$

Parameter ω_g is the PCC voltage angular frequency. \hat{V}_g and \hat{I}_L^* represent the amplitude of the PCC voltage and desired load current, respectively; and φ^* is the phase shift between the PCC voltage and injected StatCom current into the grid.

Coherent harmonic reference signals agree with the aforementioned averaged model in (10), hence,

$$\dot{\bar{\mathbf{x}}}^*(t) = \left(\mathbf{A} + \sum_{j=1}^n \mathbf{B}_j \delta_j^*(t) \right) \bar{\mathbf{x}}^*(t) + \mathbf{C} v_g(t), \quad (14)$$

where $\bar{\mathbf{x}}^* = [\bar{i}_L^* \ \bar{v}_{C_1}^* \ \bar{v}_{C_2}^* \ \dots \ \bar{v}_{C_n}^*]^T$ represents the desired averaged current and voltages. Expression (14) represents the steady-state dynamics of the converter. Therefore, coherent reference expressions are those that satisfy (14). Balanced capacitor voltage references in each phase is achieved by

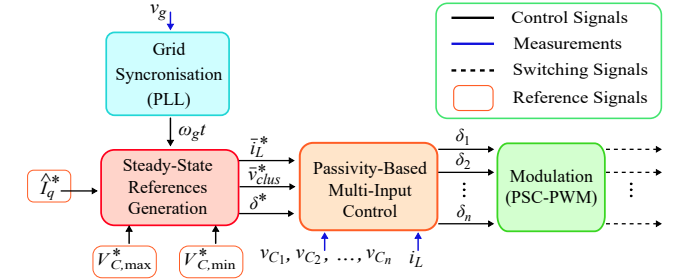


Fig. 3. Block diagram of the proposed incremental passivity-based multi-input control.

assuming $\bar{v}_{C_j}^* = \bar{v}_C^* = \bar{v}_{clus}^*/n \ \forall j \in \{1, 2, \dots, n\}$. Also, for the sake of simplicity in the reference expressions, the capacitance value C_j in each H-bridge is assumed to be equal to C , and the power losses of the H-bridges are neglected, i.e., $1/R_{SM_j} = 0$. This implies that all the reference control inputs are equal, i.e., $\delta_j^* = \delta^* \ \forall j \in \{1, 2, \dots, n\}$. Nevertheless, the extension to the asymmetric CHB multilevel converter [33] is straightforward. Although the reference control inputs are equal for all the H-bridges in the converter arm, the instantaneous errors between each capacitor voltage and its reference (balancing task) are considered in the control law derivation to calculate the individual averaged control inputs of the modulator δ_j , as explained in the next section. Consequently, the reference control input, according to the resulting reduced-order model in (14), corresponds to:

$$\delta^*(t) = \frac{L \dot{\bar{i}}_L^*(t) + R_L \bar{i}_L^*(t) + v_g(t)}{\bar{v}_{clus}^*(t)}, \quad (15)$$

when using the differential equation for the current reference. Similarly, using the differential equation for the capacitor voltage reference, the following relationship is obtained:

$$\delta^*(t) = -\frac{C \dot{\bar{v}}_{clus}^*(t)}{n \bar{i}_L^*(t)}. \quad (16)$$

Expressions (15) and (16) impose the following relationship between reference signals:

$$\frac{C}{n} \bar{v}_{clus}^*(t) \dot{\bar{v}}_{clus}^*(t) = -\bar{v}_{out}^*(t) \bar{i}_L^*(t), \quad (17)$$

where

$$\bar{v}_{out}^*(t) = L \dot{\bar{i}}_L^*(t) + R_L \bar{i}_L^*(t) + v_g(t), \quad (18)$$

represents the converter output voltage reference.

Integrating both sides of (17) yields,

$$\bar{v}_{clus}^{*2}(t) = \bar{v}_{clus}^{*2}(0) - \frac{2n}{C} \int_0^t \bar{v}_{out}^*(\tau) \bar{i}_L^*(\tau) d\tau, \quad (19)$$

where $\bar{v}_{clus}^*(0)$ is the initial condition. Note that the integrator operator is computed using known mathematical expressions, i.e., equation (18) is calculated from (12) and (13), and finally, the voltage reference corresponding to (19) is calculated from

(12) and (18). Also, it should be noted that the capacitor voltages are closely linked to the instantaneous energy in the converter arm. According to (12) and (13), (19) can be expressed as:

$$\begin{aligned} \bar{v}_{clus}^{*2}(t) = & n^2 V_{C,rms}^{*2} + \frac{nX_L \hat{I}_L^{*2}}{2\omega_g C} \cos(2\omega_g t + 2\varphi^*) \\ & - \frac{n\hat{I}_L^* \hat{V}_g}{C} \cos(\varphi^*) t + \frac{n\hat{I}_L^* \hat{V}_g}{2\omega_g C} \sin(2\omega_g t + \varphi^*) \\ & - \frac{nR_L \hat{I}_L^{*2}}{C} t + \frac{nR_L \hat{I}_L^{*2}}{2\omega_g C} \sin(2\omega_g t + 2\varphi^*), \quad (20) \end{aligned}$$

where $X_L = \omega_g L$ is the inductor reactance, and $V_{C,rms}^*$ is the rms value of the capacitor voltages (i.e., $V_{C,rms}^* = \sqrt{\frac{1}{T} \int_0^T \bar{v}^{*2}(t) dt}$). The non-periodic terms in (20) are $\frac{n\hat{I}_L^* \hat{V}_g}{C} \cos(\varphi^*) t$ and $\frac{nR_L \hat{I}_L^{*2}}{C} t$. A stationary behaviour of the power converter (i.e., there is no increment of energy in the capacitor voltages over a grid period) implies:

$$\frac{n\hat{I}_L^* \hat{V}_g}{C} \cos(\varphi^*) t + \frac{nR_L \hat{I}_L^{*2}}{C} t = 0. \quad (21)$$

Consequently, the phase shift between the injected current $\bar{i}_L^*(t)$ and the PCC voltage $v_g(t)$ is not purely reactive. In fact, this means that the phase shift, according to (21), is equal to:

$$\varphi^* = \pm \arccos\left(-\frac{R_L \hat{I}_L^*}{\hat{V}_g}\right), \quad (22)$$

or equivalently,

$$\varphi^* = \pm \frac{\pi}{2} + \alpha_v^*, \quad (23)$$

where α_v^* is the phase shift between converter output voltage reference and PCC voltage, which is determined by the losses in the converter and the operating point (see Appendix). Obviously, the circuit is not purely reactive when $R_L \neq 0$, and the phase shift φ^* takes into account the relationship between the active power, that compensates for the losses, and the apparent power drawn from the grid. Note that in this case, the magnitude of the active power current component \hat{I}_d^* and the magnitude of the reactive power current component \hat{I}_q^* correspond to:

$$\hat{I}_d^* = \hat{I}_L^* \cos(\varphi^*) \quad (24)$$

$$\hat{I}_q^* = \hat{I}_L^* \sin(\varphi^*), \quad (25)$$

respectively. Equivalently, using (22):

$$\hat{I}_d^* = -\frac{R_L \hat{I}_L^{*2}}{\hat{V}_g} \quad (26)$$

$$\hat{I}_q^* = \pm \hat{I}_L^* \sqrt{1 - \left(\frac{R_L \hat{I}_L^*}{\hat{V}_g}\right)^2}. \quad (27)$$

Note that (12) implies that it is only desired to inject a fundamental harmonic into the PCC. Nevertheless, the same procedure can be used to inject any other harmonic component required for power distortion compensation. Also, note that when the PCC voltage contains undesired harmonics, which can be measured or estimated [34]–[36], the reference signal expression in (20) will change accordingly adding two new similar terms per harmonic.

Similarly, the management of the reference expressions enables to isolate one or more H-bridges to overcome reliability problems on the switching devices or dc-link capacitors.

B. Reference Design Criteria

This subsection addresses design criteria concerning the maximum and the minimum allowable capacitor voltages, as well as the saturation of the averaged control input of the modulator. The maximum capacitor voltage is limited to the voltage rating of the converter, whilst the minimum capacitor voltage is constrained by the modulation signal saturation.

In the LC-StatCom, the magnitude of the low-frequency oscillation on the capacitor voltages is large, and the control has to ensure that the peak of this oscillation does not exceed a predetermined value $V_{C,max}^*$, which is imperative for safety issues and to not compromise the converter voltage rating. This, in turn, necessitates that the reference for the rms value of the capacitor voltages $V_{C,rms}^*$ in (20) is related with the maximum allowable capacitor voltage and with the amplitude of the injected current, as [7] describes. As analysed in [7], the reason for having a reference value for $V_{C,rms}^*$ that varies with the operating conditions is to keep the maximum voltage on the capacitors regulated to $V_{C,max}^*$ regardless of the reactive power demand.

From (20), using (22), and grouping the second harmonic terms, the capacitor voltage reference can be reformulated as:

$$\bar{v}_C^*(t) = \sqrt{V_{C,max}^{*2} - \Delta V_C^{*2} (1 \mp \cos(2\omega_g t + 2\alpha_v^*))}, \quad (28)$$

where $\Delta V_C^{*2} = \frac{\hat{I}_L^* \hat{V}_{out}^*}{2\omega_g n C}$. Note that ΔV_C^{*2} denotes the amplitude of \bar{v}_C^{*2} around $V_{C,max}^{*2} - \Delta V_C^{*2}$. This means that \bar{v}_C^{*2} has a value between $V_{C,max}^{*2}$ and $V_{C,max}^{*2} - 2\Delta V_C^{*2}$. Equation (28) is reformulated in this form because it is desired to express the reference signals as a function of the maximum allowable capacitor voltage $V_{C,max}^*$.

In the experimental results presented in the following sections, the value for the maximum allowable reference capacitor voltage is forty percent more than the PCC voltage amplitude divided by the number of H-bridges, that is $V_{C,max}^* = 1.4\hat{V}_g/n$. This choice is made to ensure that (28) is satisfied, i.e., $V_{C,max}^{*2} \geq 2\Delta V_C^{*2}$.

Ensuring that the reference control input δ^* is bounded within the range $[-1, 1]$, implies, using (15) and (18), that $n\bar{v}_C^* \geq |\bar{v}_{out}^*|$, which determines the minimum allowable capacitor voltage for a given $V_{C,\max}^*$ and \hat{I}_L^* .

For LC-StatComs under inductive operation, the sum of capacitor voltages v_{clus} , and the converter voltage v_{out} , are in opposite phase. Therefore, for large voltage oscillations, the amplitude of the converter voltage reference \hat{V}_{out}^* (see Appendix), can exceed the minimum value of the sum of capacitor voltages reference, denoted as $nV_{C,\min}^*$. Then, according to (15), the reference control input would be saturated, leading to undesired current distortion [7].

To overcome this situation, condition (29) is derived evaluating (28) at its minimum, which relates the minimum value of the sum of capacitor voltages (left-hand side) with the converter voltage amplitude during inductive operation (right-hand side),

$$n\sqrt{V_{C,\max}^{*2} - \frac{\hat{I}_L^* \hat{V}_{out}^*}{\omega_g n C}} \geq \hat{V}_{out}^*, \quad \text{with} \quad (29)$$

$$\hat{V}_{out}^* = -X_L \hat{I}_L^* + \hat{V}_g \sqrt{1 - \left(\frac{R_L \hat{I}_L^*}{\hat{V}_g}\right)^2}.$$

It can be noted that satisfying (29) guarantees that the reference control input is not saturated during inductive operating mode.

It should be noted that references for the current (12), voltage (28), and control input (15), can be easily programmed in a digital device. Next, the proposed controller based on passivity concepts, which employs these reference expressions, is described.

IV. DESIGN OF THE PASSIVITY-BASED MULTI-INPUT CONTROL

A. Incremental Dynamics

The incremental state variables $\tilde{\mathbf{x}}$ and incremental control inputs $\tilde{\delta}_j$, or error signals with respect to their references, are defined as follows:

$$\tilde{\mathbf{x}}(t) = \mathbf{x}(t) - \mathbf{x}^*(t) \quad (30)$$

$$\tilde{\delta}_j(t) = \delta_j(t) - \delta^*(t), \quad (31)$$

where $\forall j \in \{1, 2, \dots, n\}$. Then, the incremental averaged model of (10), given that the reference signals are coherent, is

$$\dot{\tilde{\mathbf{x}}}(t) = \mathbf{A}(t) \tilde{\mathbf{x}} + \sum_{j=1}^n \mathbf{B}_j(t) \tilde{\delta}_j + \sum_{j=1}^n \mathcal{B}_j \tilde{\mathbf{x}} \tilde{\delta}_j. \quad (32)$$

Thus, (32) has a nonlinear nonautonomous nature [37], where the time-varying matrices $\mathbf{A}(t) \in \mathbb{R}^{(n+1) \times (n+1)}$ and $\mathbf{B}_j(t) \in \mathbb{R}^{(n+1) \times 1}$ are defined as follows:

$$\mathbf{A}(t) = \mathcal{A} + \sum_{j=1}^n \mathcal{B}_j \delta^*(t) \quad (33)$$

$$\mathbf{B}_j(t) = \mathcal{B}_j \bar{\mathbf{x}}^*(t), \quad (34)$$

where $\forall j \in \{1, 2, \dots, n\}$. In the previous expressions, the time-dependent nature of the variables $\delta^*(t)$ and $\bar{\mathbf{x}}^*(t)$ is highlighted, whereas the time dependency of the incremental variables $\tilde{\delta}_j$ and $\tilde{\mathbf{x}}$ is avoided for the sake of brevity. It can be noted that the time-varying matrices defining the nonautonomous system in (32) are periodic and bounded, as their elements depend on the variables $\delta^*(t)$ and $\bar{\mathbf{x}}^*(t)$, which are periodic and bounded, as shown in Section III-A.

For instance, in a CHB converter case with three H-bridges, $n = 3$:

$$\mathbf{A}(t) = \begin{bmatrix} -\frac{R_L}{\delta^*(t)} & \frac{\delta^*(t)}{L} & \frac{\delta^*(t)}{L} & \frac{\delta^*(t)}{L} \\ -\frac{1}{C} & -\frac{1}{R_{SM}C} & 0 & 0 \\ -\frac{\delta^*(t)}{C} & 0 & -\frac{1}{R_{SM}C} & 0 \\ -\frac{\delta^*(t)}{C} & 0 & 0 & -\frac{1}{R_{SM}C} \end{bmatrix} \quad (35)$$

$$\mathbf{B}_1(t) = \begin{bmatrix} \frac{\bar{v}_C^*(t)}{L} \\ -\frac{\bar{i}_L^*(t)}{C} \\ 0 \\ 0 \end{bmatrix}, \quad \mathbf{B}_2(t) = \begin{bmatrix} \frac{\bar{v}_C^*(t)}{L} \\ 0 \\ -\frac{\bar{i}_L^*(t)}{C} \\ 0 \end{bmatrix},$$

$$\mathbf{B}_3(t) = \begin{bmatrix} \frac{\bar{v}_C^*(t)}{L} \\ 0 \\ 0 \\ -\frac{\bar{i}_L^*(t)}{C} \end{bmatrix}. \quad (36)$$

This case is used to corroborate the proposed control approach in the section devoted to experimental results.

B. Incremental Passivity Control Law

With the purpose of finding a control law that manages the nonlinear nonautonomous nature of the system, the following scalar candidate-Lyapunov-function (CLF) is defined:

$$V(\tilde{\mathbf{x}}) = \frac{1}{2} \tilde{\mathbf{x}}^T \mathbf{P} \tilde{\mathbf{x}}, \quad (37)$$

where $\mathbf{P} \in \mathbb{R}^{(n+1) \times (n+1)}$ is a symmetric positive definite matrix,

$$\mathbf{P} = \mathbf{P}^T = \begin{bmatrix} L & 0 & 0 & \dots & 0 \\ 0 & C_1 & 0 & \dots & 0 \\ 0 & 0 & C_2 & \dots & 0 \\ \vdots & \vdots & \vdots & \ddots & \vdots \\ 0 & 0 & 0 & \dots & C_n \end{bmatrix} > 0. \quad (38)$$

Thus, the CLF (37) can be rewritten as:

$$V(\tilde{\mathbf{x}}) = \frac{1}{2} \left(L \tilde{i}_L^2 + \sum_{j=1}^n C_j \tilde{v}_{C_j}^2 \right), \quad (39)$$

which represents a storage function of the incremental model (32) with respect to its equilibrium trajectory, that is, the incremental energy in the storage elements (inductor and capacitors). It can be noted that $V(\tilde{\mathbf{x}})$ does not depend explicitly on time, that is, the time-dependence is through the incremental state variables $\tilde{\mathbf{x}}$. Also, it can be noted that it is globally positive definite and radially unbounded, i.e.,

$$V(\tilde{\mathbf{x}}) > 0, \quad \forall \tilde{\mathbf{x}} \in \mathbb{R}^{n+1} / \tilde{\mathbf{x}} \neq \mathbf{0}, \quad (40)$$

and

$$V(\tilde{\mathbf{x}}) \rightarrow \infty, \quad \text{as } \|\tilde{\mathbf{x}}\| \rightarrow \infty, \quad (41)$$

respectively.

The time-derivative of the CLF (37) along the trajectory of the system (32), corresponds to:

$$\begin{aligned} \dot{V}(\tilde{\mathbf{x}}, t) = & \frac{1}{2} \tilde{\mathbf{x}}^T (\mathbf{A}^T(t) \mathbf{P} + \mathbf{P} \mathbf{A}(t)) \tilde{\mathbf{x}} + \sum_{j=1}^n \mathbf{B}_j^T(t) \mathbf{P} \tilde{\mathbf{x}} \tilde{\delta}_j \\ & + \frac{1}{2} \tilde{\mathbf{x}}^T \sum_{j=1}^n (\mathcal{B}_j^T \mathbf{P} + \mathbf{P} \mathcal{B}_j) \tilde{\mathbf{x}} \tilde{\delta}_j, \end{aligned} \quad (42)$$

where it can be noted that $\dot{V}(\tilde{\mathbf{x}}, t)$ does depend explicitly on t , thus the stability proof has to take into account the nonautonomous nature of the problem [37].

In (42), the first term, represented in (43), is strict negative definite:

$$\begin{aligned} & \frac{1}{2} (\mathbf{A}^T(t) \mathbf{P} + \mathbf{P} \mathbf{A}(t)) = \\ & - \begin{bmatrix} R_L & 0 & 0 & \cdots & 0 \\ 0 & \frac{1}{R_{SM1}} & 0 & \cdots & 0 \\ 0 & 0 & \frac{1}{R_{SM2}} & \cdots & 0 \\ \vdots & \vdots & \vdots & \ddots & \vdots \\ 0 & 0 & 0 & \cdots & \frac{1}{R_{SMn}} \end{bmatrix} < 0. \end{aligned} \quad (43)$$

Furthermore, the third term, as represented in (44), is always zero:

$$\frac{1}{2} (\mathcal{B}_j^T \mathbf{P} + \mathbf{P} \mathcal{B}_j) = \mathbf{0}, \quad (44)$$

where $\forall j \in \{1, 2, \dots, n\}$.

Therefore, the time-derivative of the CLF satisfies:

$$\dot{V}(\tilde{\mathbf{x}}, t) \leq \sum_{j=1}^n \mathbf{B}_j^T(t) \mathbf{P} \tilde{\mathbf{x}} \tilde{\delta}_j, \quad (45)$$

which considers the lossless case, where $R_L = 0$ and $1/R_{SMj} = 0$. Therefore, it can be concluded that $V(\tilde{\mathbf{x}})$ represents a Lyapunov function for the system (32).

The n feedback outputs can be defined as:

$$y_j(t) = \mathbf{B}_j^T(t) \mathbf{P} \tilde{\mathbf{x}} = \tilde{\mathbf{x}}^T \mathbf{P} \mathbf{B}_j(t), \quad (46)$$

where $\forall j \in \{1, 2, \dots, n\}$, that can be rewritten in terms of the incremental state variables as,

$$y_j(t) = \bar{v}_C^*(t) \tilde{i}_L - \bar{i}_L^*(t) \tilde{v}_{Cj}, \quad (47)$$

or equivalently, using (30), y_j can be expressed in terms of average state variables as,

$$y_j(t) = \bar{v}_C^*(t) \bar{i}_L - \bar{i}_L^*(t) \bar{v}_{Cj}. \quad (48)$$

Therefore, the time-derivative of the Lyapunov function fulfills:

$$\dot{V}(\tilde{\mathbf{x}}, t) \leq \sum_{j=1}^n y_j(t) \tilde{\delta}_j. \quad (49)$$

It is noted that (49) corresponds to a passive relationship between feedback output y_j and incremental control input $\tilde{\delta}_j$ [37], [38]. Thus, by feeding back the j^{th} output y_j times a constant positive gain α , which means that the feedback control law is

$$\tilde{\delta}_j(t) = -\alpha y_j(t), \quad \text{with constant } \alpha > 0, \quad (50)$$

where $\forall j \in \{1, 2, \dots, n\}$, the time-derivative of the Lyapunov function becomes globally negative semi-definite,

$$\dot{V}(\tilde{\mathbf{x}}, t) = -\alpha \sum_{j=1}^n (\bar{v}_C^*(t) \tilde{i}_L - \bar{i}_L^*(t) \bar{v}_{Cj})^2 \leq 0. \quad (51)$$

Note that when $R_L \neq 0$ and $1/R_{SMj} \neq 0$, $\dot{V}(\tilde{\mathbf{x}}, t) < 0$, which proves that the incremental dynamics tend to zero. Consequently, the system is globally asymptotically stable and it tends towards the aforementioned references in (12) and (28).

In the lossless case, where $R_L = 0$ and $1/R_{SMj} = 0$, the time-derivative of the Lyapunov function is negative semi-definite, i.e., $\dot{V}(\tilde{\mathbf{x}}, t) \leq 0$. Therefore, the uniform stability of the system can be studied using Barbalat's lemma (page 123 of [37]), and the lemma of page 125 of [37]. Given that $V(\tilde{\mathbf{x}})$ is lower bounded and that $\dot{V}(\tilde{\mathbf{x}}, t)$ is negative semi-definite, and in addition, it can be checked that $\dot{V}(\tilde{\mathbf{x}}, t)$ is uniformly continuous in time (i.e., $\ddot{V}(\tilde{\mathbf{x}}, t)$ is bounded), it can be concluded that $\dot{V}(\tilde{\mathbf{x}}, t) \rightarrow 0$ as $t \rightarrow \infty$, or equivalently, that $y_j(t) \rightarrow 0$ as $t \rightarrow \infty$. The asymptotic stability for the lossless case can be proved by using the concept of positive limit sets for nonautonomous periodic systems, as discussed in [38] (see [39] for a detailed demonstration).

It can be noted that even though the nonlinear nature of the LC-StatCom is considered in the derivations, the derived control law is linear.

It is worth to mention, that due to the saturation in the averaged control input of the modulator δ_j , the incremental control input $\tilde{\delta}_j$ must belong to the interval:

$$-1 - \delta^*(t) \leq \tilde{\delta}_j(t) \leq 1 - \delta^*(t), \quad (52)$$

where $\forall j \in \{1, 2, \dots, n\}$.

The saturation effect can be modeled as if α behaves as a positive time-invariant nonlinear memoryless function [40]. This means that $\dot{V}(\tilde{\mathbf{x}}, t)$ is negative semi-definite regardless of the specific value of the positive constant gain α . This corroborates that the proposed passivity-based control drives the LC-StatCom to its reference despite the saturation in the incremental control input.

Now, the controller parameter α selection criteria to achieve a fast transient is studied using the following approach. Substituting the feedback control law $\tilde{\delta}_j$ into the incremental dynamics in (32), the following bilinear time-varying closed-loop dynamics is obtained:

$$\dot{\tilde{\mathbf{x}}}(t) = \left(\mathbf{A}(t) - \alpha \sum_{j=1}^n \mathbf{B}_j(t) \mathbf{B}_j^T(t) \mathbf{P} \right) \tilde{\mathbf{x}} - \alpha \sum_{j=1}^n \mathbf{B}_j \tilde{\mathbf{x}} \mathbf{B}_j^T(t) \mathbf{P} \tilde{\mathbf{x}}, \quad (53)$$

which leads to the following time-derivative for $V(\tilde{\mathbf{x}})$:

$$\dot{V}(\tilde{\mathbf{x}}, t) = \tilde{\mathbf{x}}^T \mathbf{Q}(t) \tilde{\mathbf{x}}, \quad (54)$$

with

$$\mathbf{Q}(t) = \frac{1}{2} (\mathbf{A}^T(t) \mathbf{P} + \mathbf{P} \mathbf{A}(t)) - \alpha \mathbf{P} \left(\sum_{j=1}^n \mathbf{B}_j(t) \mathbf{B}_j^T(t) \right) \mathbf{P}. \quad (55)$$

Note that $\mathbf{Q}(t)$ for the lossless case can be expressed as:

$$\mathbf{Q}(t) = -\alpha \begin{bmatrix} n\bar{v}_C^{*2} & -\bar{i}_L^* \bar{v}_C^* & -\bar{i}_L^* \bar{v}_C^* & \cdots & -\bar{i}_L^* \bar{v}_C^* \\ -\bar{i}_L^* \bar{v}_C^* & \bar{i}_L^{*2} & 0 & \cdots & 0 \\ -\bar{i}_L^* \bar{v}_C^* & 0 & \bar{i}_L^{*2} & \cdots & 0 \\ \vdots & \vdots & \vdots & \ddots & \vdots \\ -\bar{i}_L^* \bar{v}_C^* & 0 & 0 & \cdots & \bar{i}_L^{*2} \end{bmatrix}, \quad (56)$$

where the time dependence notation is avoided for the sake of simplicity and readability.

In the same way that the matrix \mathbf{P} is related with the incremental energy, the matrix $\mathbf{Q}(t)$ is related with the incremental dissipated power. The terms of $\mathbf{Q}(t)$ change at every instant of the reference trajectory. Considering, now, a set of M time-instants t_m equally spaced along a time period T , the average of each term of $\mathbf{Q}(t)$ in the considered set, corresponds to

$$\langle \mathbf{Q} \rangle = -\alpha \begin{bmatrix} n \langle \bar{v}_C^{*2} \rangle & -\langle \bar{i}_L^* \bar{v}_C^* \rangle & -\langle \bar{i}_L^* \bar{v}_C^* \rangle & \cdots & -\langle \bar{i}_L^* \bar{v}_C^* \rangle \\ -\langle \bar{i}_L^* \bar{v}_C^* \rangle & \langle \bar{i}_L^{*2} \rangle & 0 & \cdots & 0 \\ -\langle \bar{i}_L^* \bar{v}_C^* \rangle & 0 & \langle \bar{i}_L^{*2} \rangle & \cdots & 0 \\ \vdots & \vdots & \vdots & \ddots & \vdots \\ -\langle \bar{i}_L^* \bar{v}_C^* \rangle & 0 & 0 & \cdots & \langle \bar{i}_L^{*2} \rangle \end{bmatrix}, \quad (57)$$

where $\langle \bar{v}_C^{*2} \rangle$, $\langle \bar{i}_L^{*2} \rangle$, and $\langle \bar{i}_L^* \bar{v}_C^* \rangle$, represent, respectively,

$$\begin{aligned} \langle \bar{v}_C^{*2} \rangle &= \frac{1}{M} \sum_{m=0}^M \bar{v}_C^{*2}[m], \\ \langle \bar{i}_L^{*2} \rangle &= \frac{1}{M} \sum_{m=0}^M \bar{i}_L^{*2}[m], \\ \langle \bar{i}_L^* \bar{v}_C^* \rangle &= \frac{1}{M} \sum_{m=0}^M \bar{i}_L^* \bar{v}_C^*[m], \end{aligned} \quad (58)$$

where $\bar{v}_C^{*2}[m] = \bar{v}_C^{*2}(t_m)$, $\bar{i}_L^{*2}[m] = \bar{i}_L^{*2}(t_m)$, and $\bar{i}_L^* \bar{v}_C^*[m] = \bar{i}_L^* \bar{v}_C^*(t_m)$. As $\bar{i}_L^*(t) \bar{v}_C^*(t)$ is a symmetric bounded signal, $\langle \bar{i}_L^* \bar{v}_C^* \rangle = 0$. Thus, (57) can be rewritten as

$$\langle \mathbf{Q} \rangle = -\alpha \begin{bmatrix} n \langle \bar{v}_C^{*2} \rangle & 0 & 0 & \cdots & 0 \\ 0 & \langle \bar{i}_L^{*2} \rangle & 0 & \cdots & 0 \\ 0 & 0 & \langle \bar{i}_L^{*2} \rangle & \cdots & 0 \\ \vdots & \vdots & \vdots & \ddots & \vdots \\ 0 & 0 & 0 & \cdots & \langle \bar{i}_L^{*2} \rangle \end{bmatrix}. \quad (59)$$

Note that when M is large enough, $\langle \bar{i}_L^{*2} \rangle$ corresponds with the square rms value of $\bar{i}_L^*(t)$, and similarly for $\langle \bar{v}_C^{*2} \rangle$. Thus, (59) can be rewritten as

$$\langle \mathbf{Q} \rangle = -\alpha \begin{bmatrix} nV_{C,rms}^{*2} & 0 & 0 & \cdots & 0 \\ 0 & \hat{I}_{L,rms}^{*2} & 0 & \cdots & 0 \\ 0 & 0 & \hat{I}_{L,rms}^{*2} & \cdots & 0 \\ \vdots & \vdots & \vdots & \ddots & \vdots \\ 0 & 0 & 0 & \cdots & \hat{I}_{L,rms}^{*2} \end{bmatrix}. \quad (60)$$

Now, invoking the convergence lemma in page 91 of [37], which says that if a real function $V(\tilde{\mathbf{x}})$ satisfies the inequality

$$\dot{V}(\tilde{\mathbf{x}}, t) + \gamma V(\tilde{\mathbf{x}}) \leq 0, \quad (61)$$

where γ is a real positive number. Then,

$$V(\tilde{\mathbf{x}}(t)) \leq V(\tilde{\mathbf{x}}(0)) e^{-\gamma t}, \quad (62)$$

which means that the stored energy in the incremental model converges exponentially, with γ as its decay rate, and $\tilde{\mathbf{x}}(0)$ as the initial state. It should be noted that since $V(\tilde{\mathbf{x}})$ is a quadratic function of the incremental state-space variables, the decay constant of these variables is $\gamma/2$. Based on the previous discussion, the differential inequality in (61) can be formulated as follows:

$$\tilde{\mathbf{x}}^T \left(\mathbf{Q}(t) + \frac{\gamma}{2} \mathbf{P} \right) \tilde{\mathbf{x}} \leq 0. \quad (63)$$

Substituting $\mathbf{Q}(t)$ by its average value $\langle \mathbf{Q} \rangle$, (63) can be rewritten as

$$\tilde{\mathbf{x}}^T \left(\langle \mathbf{Q} \rangle + \frac{\gamma}{2} \mathbf{P} \right) \tilde{\mathbf{x}} \leq 0, \quad (64)$$

which implies that

$$\alpha \geq \max \left\{ \frac{\gamma L}{2nV_{C,rms}^{*2}}, \frac{\gamma C}{2\hat{I}_{L,rms}^{*2}} \right\}. \quad (65)$$

Therefore, it can be concluded that if α fulfills (65), one can guarantee an average value for the decay rate γ over the

TABLE I
 PARAMETERS OF THE EXPERIMENTAL SETUP

Definition	Symbol	Value
PCC Voltage Nominal Amplitude	\hat{V}_g	$200\sqrt{2}$ V (1 p.u.)
Nominal Power	S_g	1 kVA (1 p.u.)
Number of H-Bridges per Arm	n	3
Grid Frequency	f_g	50 Hz
Peak Capacitor Voltage Reference	$V_{C,\max}^*$	132 V
Capacitance per H-Bridge	C	0.18 mF (0.442 p.u.)
Interface Filter Inductance	L	5 mH (0.044 p.u.)
Parasitic Parameter	R_L	0.2 Ω
Decay Rate	γ	150

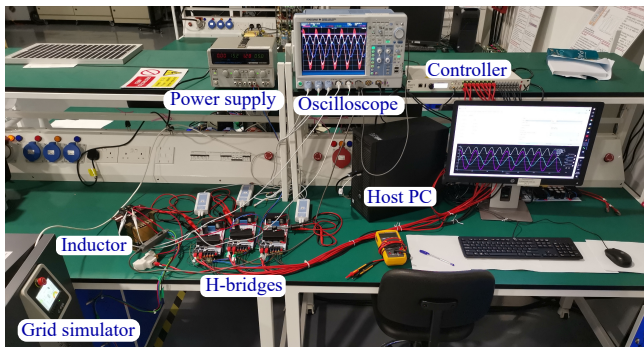


Fig. 4. Experimental setup.

set of M time-instants. Particularly, in the paper, the following value for the α parameter has been chosen

$$\alpha = \max \left\{ \frac{\gamma L}{2nV_{C,\text{rms}}^*}, \frac{\gamma C}{2\hat{I}_{L,\text{rms}}^*} \right\}, \quad (66)$$

which ensures an average decay rate higher or equal than γ . Obviously, the actual decay rate depends on the particular instant where the perturbation occurs.

V. EXPERIMENTAL RESULTS

With the purpose of illustrating the feasibility and good performance of the proposed passivity-based multi-input control law, experimental results are obtained on a 1-kVA scaled-down CHB converter arm with three H-bridges (see Fig. 4). The PCC voltage is provided by a GE&EL 15 kVA CINERGIA grid emulator. IMPERIX PEH2015 H-bridge modules are used, which are connected in series to form the seven-level converter. The parameters of the scaled-down LC-StatCom prototype are shown in Table I. It can be appreciated that the size of the capacitors C is relatively small, which results in approximately 70% (of the nominal dc component) low-frequency voltage oscillation magnitude at the rated power. The control scheme

depicted in Fig. 3 is implemented using a BOOMBOX RCP board from IMPERIX. PSC-PWM is implemented in the controller [29], [30], which generates a constant switching firing pulse pattern in the converter.

The various features of the proposed control algorithm are evaluated on the LC-StatCom CHB converter with three different test cases: *Case I*: Balancing capability considering an initial unbalanced capacitor voltage state, *Case II*: Steady-state operation, and *Case III*: Transient response.

Case I: Balancing capability considering an initial unbalanced capacitor voltage state, specifically, $\bar{v}_{C_1}^* = 1.5\bar{v}_{clus}^*/n$, $\bar{v}_{C_2}^* = 0.5\bar{v}_{clus}^*/n$, and $\bar{v}_{C_3}^* = \bar{v}_{clus}^*/n$. Fig. 5 shows the experimental balancing behaviour when the converter draws (a) 33% rated capacitive power, and (b) 100% rated capacitive power. It can be appreciated that the control reestablishes a balanced state in less than 70 ms under these test conditions. The proposed multi-input control strategy achieves accurate and fast capacitor voltage balance. As it can be observed, the higher the power processed, the faster the controller reestablishes the balancing situation. This is because the term $\bar{i}_L^* \tilde{v}_{Cj}$ in the control law (50) is proportional to the injected power, thus leading to faster control actions when \bar{i}_L^* increases.

Case II: The performance of the proposed approach in steady-state under full capacitive current is evaluated and the results are shown in Fig. 6. These waveforms exhibit 70% peak-to-peak low-frequency voltage oscillation on the capacitors. Experimental waveforms have shown a total harmonic distortion (THD) of 3.17% in the injected current into the grid. As stated in the introduction, the synthesized PWM voltage by the power converter v_{out} is shaped close to sinusoidal by the capacitor voltages when the LC-StatCom operates at 100% capacitive power, as shown as CH4 in Fig. (6).

Case III: Transient behaviours are illustrated in Fig. 7, which depicts the experimental waveforms under sudden change of the reactive power level reference. Specifically, Fig. 7 depicts the transient waveforms in (a) capacitive mode during a change from 33%-rated power to full-rated power, and (b) the transition from full-rated power capacitive-mode to 33%-rated power inductive-mode. It can be noted that the transient response is very fast, while correct voltage balancing and peak regulation of the capacitor voltages are also obtained after the occurrence of the transient. The proposed control is able to reach a perfect global tracking of the time-varying reference signals in less than 5 ms.

In Fig. 7(b), it can be appreciated that the control of the injected current is lost, due to the saturation of the averaged control input of the modulator (i.e., $v_{clus} \geq |\bar{v}_{out}^*|$). The energy stored in the inductor needs to be suddenly reduced, whilst the capacitive energy stored in the capacitors needs to be increased. The proposed controller uses this excess of energy in the inductor to charge the capacitors accordingly. This inherent exchange of energy within the inductor and the capacitors represents the key of the proposed control approach, which illustrates that there is sufficient stored energy in the LC-StatCom to have fast and smooth transitions between operating modes. On the other hand, in a conventional cascade

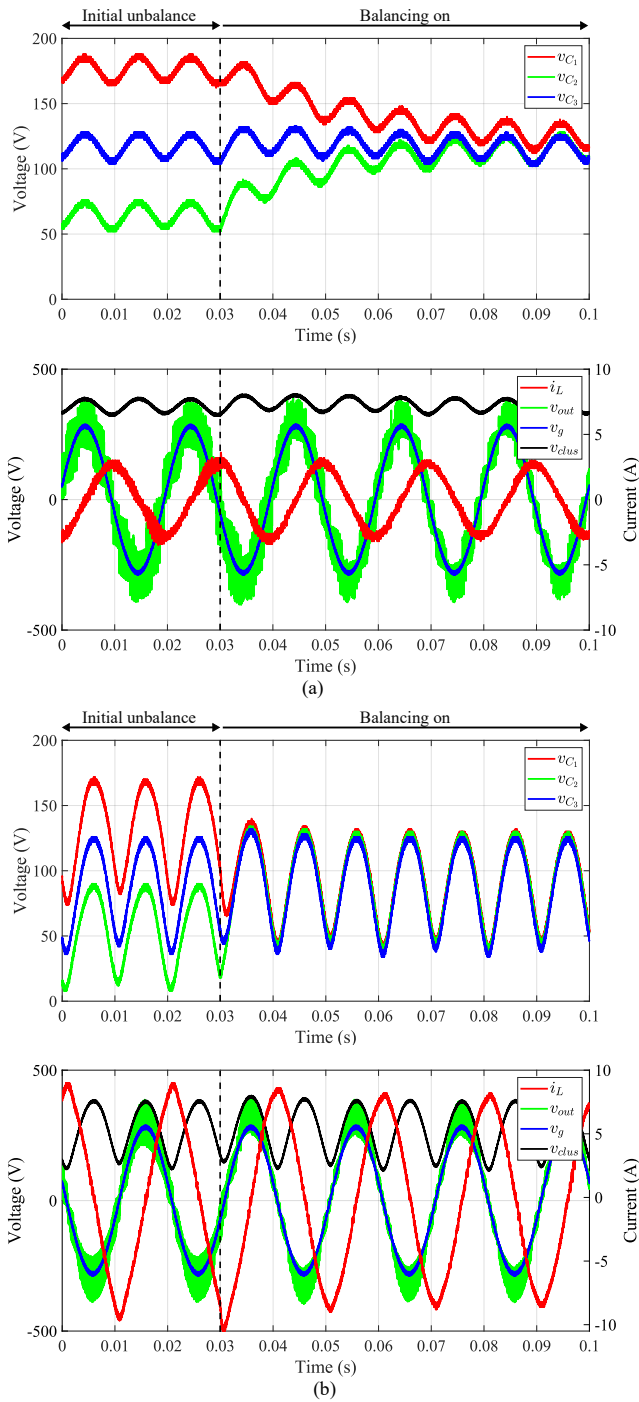


Fig. 5. **Case I:** Experimental waveforms showing the balancing capability when operating the LC-StatCom at (a) 33% capacitive operation, and (b) 100% capacitive operation.

control structure, such as those in [7], [12], and illustrated in Fig. 1(b), the outer voltage control loop initially requests relatively high active power current component to the grid (\hat{I}_d^*) in order to charge the capacitor voltages. This phenomena takes place unavoidably due to the cascade structure of the control. Therefore, whether there is enough energy stored in the inductor to charge the capacitors is not taken into

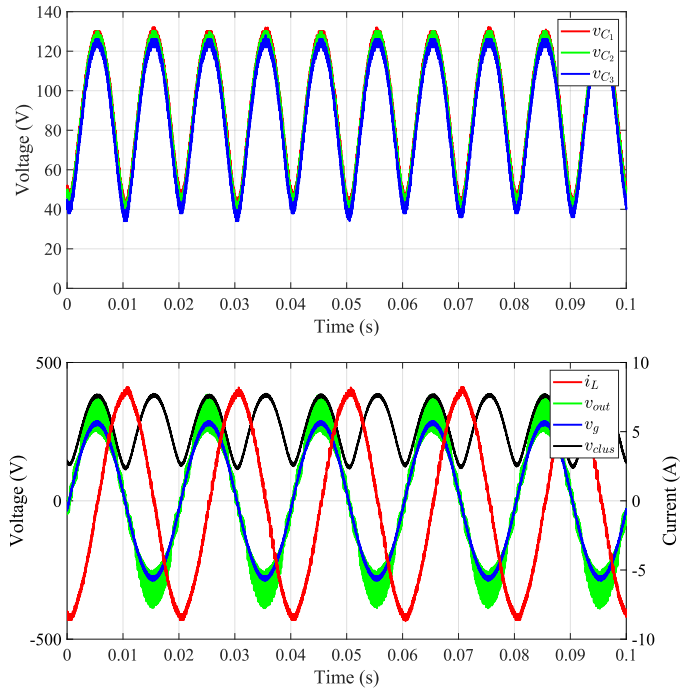


Fig. 6. **Case II:** Experimental waveforms showing the steady-state performances when operating the LC-StatCom at 100% capacitive operation.

account by the controller, which disturbs the grid unnecessarily demanding extra active power during the transient. Once the cluster voltage reaches its reference, the required active power component drops to the value that only compensates for the losses.

VI. CONCLUSION

An incremental passivity-based multi-input control law has been developed for LC-StatComs. The paper has reviewed the multivariate averaged model of the converter that takes into account its bilinear nature. Using this multivariate bilinear model, which is time-varying, it analyses a set of coherent reference signals to be tracked. These tracking signals ensure a prescribed capacitor voltage limit, besides ensuring that the reference control inputs are in the range $[-1, 1]$. Then, the paper develops a multi-input incremental passivity law that guarantees global tracking of the specified references and balances the capacitor voltages despite saturations in the averaged control inputs of the modulator. From the incremental passivity control derivation, it results in a linear periodically time-varying law easily implementable with standard digital controllers. The paper also shows a comprehensive set of experimental measures that corroborates the excellent behaviour of the proposed approach. Experimental results exhibit fast balancing responses, fast transients between operating modes, and low harmonic distortion in the injected StatCom current, showing agreement with expected theoretical performances.

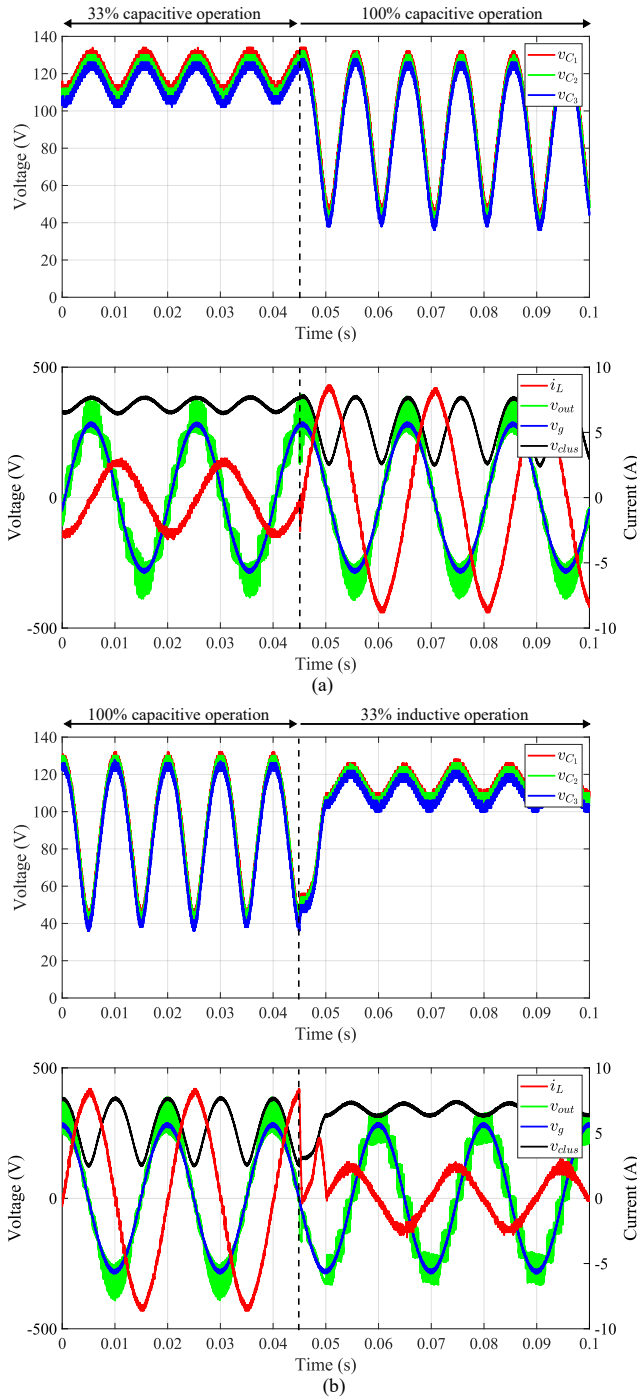


Fig. 7. **Case III:** Experimental waveforms during a sudden reactive power change (a) from 33% capacitive operation to 100% capacitive operation, and (b) from 100% capacitive operation to 33% inductive operation.

VII. ACKNOWLEDGMENT

This work was supported by the Singapore Ministry of Education Academic Research Fund Tier 1 under Grant No: 2017-T1-001-213 (RG 90/17).

APPENDIX

ANALYTICAL EXPRESSION FOR CONVERTER VOLTAGE REFERENCE IN (18)

According to (12) and (13), (18) can be expressed in the following rectangular notation:

$$\begin{aligned} \bar{v}_{out}^*(t) = & \underbrace{\left(\hat{V}_g - X_L \hat{I}_L^* \sin(\varphi^*) + R_L \hat{I}_L^* \cos(\varphi^*) \right)}_{\hat{V}_{out,d}^*} \sin(\omega_g t) \\ & + \underbrace{\left(X_L \hat{I}_L^* \cos(\varphi^*) + R_L \hat{I}_L^* \sin(\varphi^*) \right)}_{\hat{V}_{out,q}^*} \cos(\omega_g t), \quad (67) \end{aligned}$$

which is easy to translate to its equivalent polar representation as:

$$\bar{v}_{out}^*(t) = \hat{V}_{out}^* \sin(\omega_g t + \alpha_v^*), \quad (68)$$

where

$$\hat{V}_{out}^* = \sqrt{\hat{V}_{out,d}^{*2} + \hat{V}_{out,q}^{*2}} \quad (69)$$

$$\alpha_v^* = \text{atan2} \left(\hat{V}_{out,q}^*, \hat{V}_{out,d}^* \right). \quad (70)$$

Using (22) in (67), the amplitude of the converter output voltage reference (69) is equal to

$$\hat{V}_{out}^* = -X_L \hat{I}_L^* + \hat{V}_g \sqrt{1 - \left(\frac{R_L \hat{I}_L^*}{\hat{V}_g} \right)^2} \quad (71)$$

during inductive operation (i.e., when $\varphi^* = \frac{\pi}{2} + \alpha_v^*$), whereas it is

$$\hat{V}_{out}^* = X_L \hat{I}_L^* + \hat{V}_g \sqrt{1 - \left(\frac{R_L \hat{I}_L^*}{\hat{V}_g} \right)^2} \quad (72)$$

during capacitive operation (i.e., when $\varphi^* = -\frac{\pi}{2} + \alpha_v^*$). It is worth noting that the total voltage \hat{V}_{out}^* , which the converter needs to generate, is greater than the PCC voltage magnitude \hat{V}_g during capacitive operation (72), and less than \hat{V}_g during inductive operation (71).

REFERENCES

- [1] J. Dixon, L. Moran, J. Rodriguez, and R. Domke, "Reactive power compensation technologies: state-of-the-art review," vol. 93, pp. 2144–2164, Dec. 2005.
- [2] B. Singh, R. Saha, A. Chandra, and K. Al-Haddad, "Static synchronous compensators (STATCOM): A review," *IET Power Electronics*, vol. 2, no. 4, pp. 297–324, Jul. 2009.
- [3] P. Westcott and C. Candelise, "Assessing the impacts of photovoltaic penetration across an entire low-voltage distribution network containing 1.5 million customers," *IET Renewable Power Generation*, vol. 10, no. 4, pp. 460–466, Jan. 2016.

- [4] M. Hasheminamin, V. G. Agelidis, V. Salehi, R. Teodorescu, and B. Hredzak, "Index-based assessment of voltage rise and reverse power flow phenomena in a distribution feeder under high PV penetration," *IEEE Journal of Photovoltaics*, vol. 5, no. 4, pp. 1158–1168, Jul. 2015.
- [5] J. I. Leon, S. Vazquez, and L. G. Franquelo, "Multilevel converters: Control and modulation techniques for their operation and industrial applications," *Proc. of the IEEE*, vol. 105, no. 11, pp. 2066–2081, Nov. 2017.
- [6] K. Sano and M. Takasaki, "A transformerless D-STATCOM based on a multivoltage cascade converter requiring no dc sources," *IEEE Trans. Power Electron.*, vol. 27, no. 6, pp. 2783–2795, Jun. 2012.
- [7] G. Farivar, C. D. Townsend, B. Hredzak, J. Pou, and V. G. Agelidis, "Low-capacitance cascaded H-bridge multilevel StatCom," *IEEE Trans. Power Electron.*, vol. 32, no. 3, pp. 1744–1754, Mar. 2017.
- [8] T. Isobe, D. Shiojima, K. Kato, Y. R. R. Hernandez, and R. Shimada, "Full-bridge reactive power compensator with minimized-equipped capacitor and its application to static var compensator," *IEEE Trans. Power Electron.*, vol. 31, no. 1, pp. 224–234, Jan. 2016.
- [9] G. Farivar, B. Hredzak, and V. G. Agelidis, "Reduced-capacitance thin-film H-bridge multilevel STATCOM control utilizing an analytic filtering scheme," *IEEE Trans. Ind. Electron.*, vol. 62, no. 10, pp. 6457–6468, Oct. 2015.
- [10] G. Farivar, C. D. Townsend, B. Hredzak, J. Pou, and V. G. Agelidis, "Passive reactor compensated cascaded H-bridge multilevel LC-StatCom," *IEEE Trans. Power Electron.*, vol. 32, no. 11, pp. 8338–8348, Nov. 2017.
- [11] Z. He, L. Zhang, T. Isobe, and H. Tadano, "Dynamic performance improvement of single-phase STATCOM with drastically reduced capacitance," in *Proc. IEEE 3rd Intern. Future Energy Electron. Conf. and ECCE Asia (IFEEC 2017 - ECCE Asia)*, pp. 1413–1418, Jun. 2017.
- [12] T. Isobe, L. Zhang, H. Tadano, J. A. Suul, and M. Molinas, "Control of DC-capacitor peak voltage in reduced capacitance single-phase STATCOM," in *Proc. IEEE 17th Workshop on Control and Modeling for Power Electron. (COMPEL)*, pp. 1–8, Jun. 2016.
- [13] H. Wang and F. Blaabjerg, "Reliability of capacitors for DC-link applications in power electronic converters - An overview," *IEEE Trans. Ind. Appl.*, vol. 50, no. 5, pp. 3569–3578, Sep. 2014.
- [14] B. Karanayil, V. G. Agelidis, and J. Pou, "Evaluation of dc-link decoupling using electrolytic or polypropylene film capacitors in three-phase grid-connected photovoltaic inverters," in *Proc. IECON 2013 - 39th Annual Conference of the IEEE Industrial Electronics Society*, pp. 6980–6986, Nov. 2013.
- [15] R. Maheshwari, S. Munk-Nielsen, and S. Busquets-Monge, "Design of neutral-point voltage controller of a three-level NPC inverter with small DC-link capacitors," *IEEE Transactions on Industrial Electronics*, vol. 60, no. 5, pp. 1861–1871, May 2013.
- [16] G. Farivar, J. Pou, and A. Tripathi, "LC-StatCom with symmetrical I-V characteristic - power loss analysis," in *Proc. 19th European Conf. on Power Electron. and Appl. (EPE'17 ECCE Europe)*, pp. 1–10, Sep. 2017.
- [17] G. Farivar, J. Pou, and A. T., "LC-StatCom with symmetrical I-V characteristic: Total harmonic distortion study," in *Proc. Asian Conf. on Energy, Power and Transportation Electrification (ACEPT)*, pp. 1–5, Oct. 2017.
- [18] G. Farivar, B. Hredzak, and V. G. Agelidis, "Decoupled control system for cascaded H-bridge multilevel converter based STATCOM," *IEEE Trans. Ind. Electron.*, vol. 63, no. 1, pp. 322–331, Jan. 2016.
- [19] L. Harnefors, A. Antonopoulos, S. Norrga, L. Angquist, and H. Nee, "Dynamic analysis of modular multilevel converters," *IEEE Trans. Ind. Electron.*, vol. 60, no. 7, pp. 2526–2537, Jul. 2013.
- [20] C. D. Townsend, R. A. Baracarte, Y. Yu, D. Tormo, H. Z. de La Parra, G. D. Demetriades, and V. G. Agelidis, "Heuristic model predictive modulation for high-power cascaded multilevel converters," *IEEE Trans. Ind. Electron.*, vol. 63, no. 8, pp. 5263–5275, Aug. 2016.
- [21] R. Darus, J. Pou, G. Konstantinou, S. Ceballos, R. Picas, and V. G. Agelidis, "A modified voltage balancing algorithm for the modular multilevel converter: Evaluation for staircase and phase-disposition PWM," *IEEE Trans. Power Electron.*, vol. 30, no. 8, pp. 4119–4127, Aug. 2015.
- [22] S. R. Sanders, *Nonlinear control of switching power converters*. PhD thesis, Massachusetts Institute of Technology, 1989.
- [23] R. Leyva, A. Cid-Pastor, C. Alonso, I. Queindec, S. Tarbouriech, and L. Martinez-Salamero, "Passivity-based integral control of a boost converter for large-signal stability," *IEE Proceedings - Control Theory and Applications*, vol. 153, no. 2, pp. 139–146, Mar. 2006.
- [24] G. Escobar, R. Ortega, H. Sira-Ramirez, J. P. Vilain, and I. Zein, "An experimental comparison of several nonlinear controllers for power converters," *IEEE Control Systems Magazine*, vol. 19, no. 1, pp. 66–82, Feb. 1999.
- [25] R. Cisneros, M. Pirro, G. Bergna, R. Ortega, G. Ippoliti, and M. Molinas, "Global tracking passivity-based PI control of bilinear systems: Application to the interleaved boost and modular multilevel converters," *Control Engineering Practice*, vol. 43, pp. 109–119, Oct. 2015.
- [26] G. Bergna-Diaz, D. Zonetti, S. Sanchez, R. Ortega, and E. Tedeschi, "PI passivity-based control and performance analysis of MMC multi-terminal HVDC systems," *IEEE J. Emerg. Sel. Topics Power Electron.*, pp. 1–1, 2018.
- [27] R. Xu, Y. Yu, R. Yang, G. Wang, D. Xu, B. Li, and S. Sui, "A novel control method for transformerless H-bridge cascaded STATCOM with star configuration," *IEEE Trans. Power Electron.*, vol. 30, no. 3, pp. 1189–1202, Mar. 2015.
- [28] R. R. Mohler, *Bilinear control processes: with applications to engineering, ecology and medicine*. Academic Press, Inc., 1973.
- [29] C. D. Townsend, T. J. Summers, and R. E. Betz, "Phase-shifted carrier modulation techniques for cascaded h-bridge multilevel converters," *IEEE Trans. Ind. Electron.*, vol. 62, no. 11, pp. 6684–6696, Nov. 2015.
- [30] D. G. Holmes and T. A. Lipo, *Pulse width modulation for power converters: principles and practice*, vol. 18. John Wiley & Sons, 2003.
- [31] D. E. Quevedo, R. P. Aguilera, M. A. Perez, P. Cortes, and R. Lizana, "Model predictive control of an AFE rectifier with dynamic references," *IEEE Trans. Power Electron.*, vol. 27, no. 7, pp. 3128–3136, Jul. 2012.
- [32] A. Lopez, D. E. Quevedo, R. Aguilera, T. Geyer, and N. Oikonomou, "Reference design for predictive control of modular multilevel converters," in *Proc. 2014 4th Australian Control Conference (AUCC)*, pp. 239–244, Nov. 2014.
- [33] M. A. Perez, P. Cortes, and J. Rodriguez, "Predictive control algorithm technique for multilevel asymmetric cascaded H-bridge inverters," *IEEE Trans. Ind. Electron.*, vol. 55, no. 12, pp. 4354–4361, Dec. 2008.
- [34] S. Vazquez, J. A. Sanchez, M. R. Reyes, J. I. Leon, and J. M. Carrasco, "Adaptive vectorial filter for grid synchronization of power converters under unbalanced and/or distorted grid conditions," *IEEE Trans. Ind. Electron.*, vol. 61, no. 3, pp. 1355–1367, Mar. 2014.
- [35] P. Rodriguez, A. Luna, I. Candela, R. Mujal, R. Teodorescu, and F. Blaabjerg, "Multiresonant frequency-locked loop for grid synchronization of power converters under distorted grid conditions," *IEEE Trans. Ind. Electron.*, vol. 58, no. 1, pp. 127–138, Jan. 2011.
- [36] P. Rodriguez, J. Pou, J. Bergas, J. I. Candela, R. P. Burgos, and D. Boroyevich, "Decoupled double synchronous reference frame PLL for power converters control," *IEEE Trans. Power Electron.*, vol. 22, no. 2, pp. 584–592, Mar. 2007.
- [37] J.-J. E. Slotine, W. Li, *et al.*, *Applied nonlinear control*, vol. 199. Prentice hall Englewood Cliffs, NJ, 1991.
- [38] H. K. Khalil, *Nonlinear systems*, vol. 3. Prentice hall Upper Saddle River, NJ, 2002.
- [39] N. Rouche, P. Habets, I. Physiology, and M. LaLoy, *Stability Theory by Liapunov's Direct Method*. Applied mathematical sciences, 3Island Press, 1977.
- [40] R. Leyva, L. Martinez-Salamero, H. Valderrama-Blavi, J. Maixe, R. Giral, and F. Guinjoan, "Linear state-feedback control of a boost converter for large-signal stability," *IEEE Trans. Circuits Syst. I. Fundam. Theory Appl.*, vol. 48, no. 4, pp. 418–424, Apr. 2001.